Nucleic Acids Research, 2005, Vol. 33, No. 2 ***497–510***
doi:10.1093/nar/gki192

Preferential binding and structural distortion by Fe^{2+} at RGGG-containing DNA sequences correlates with enhanced oxidative cleavage at such sequences

Priyamvada Rai[2], David E. Wemmer[2,3] and Stuart Linn[1,2,*]

[1]Department of Molecular and Cell Biology, Barker Hall, University of California Berkeley, CA 94720-3202, USA, [2]Biophysics Graduate Group and [3]Department of Chemistry, University of California Berkeley, USA

Received October 18, 2004; Revised and Accepted December 23, 2004

ABSTRACT

Certain DNA sequences are known to be unusually sensitive to nicking via the Fe^{2+}-mediated Fenton reaction. Most notable are a purine nucleotide followed by three or more G residues, RGGG, and purine nucleotides flanking a TG combination, RTGR. Our laboratory previously demonstrated that nicking in the RGGG sequences occurs preferentially 5′ to a G residue with the nicking probability decreasing from the 5′ to 3′end of these sequences. Using ^1H NMR to characterize Fe^{2+} binding within the duplex CGAGTTAGGGTAGC/GCTACCCTAACTCG and 7-deazaguanine-containing (Z) variants of it, we show that Fe^{2+} binds preferentially at the GGG sequence, most strongly towards its 5′ end. Substitutions of individual guanines with Z indicate that the high affinity Fe^{2+} binding at AGGG involves two adjacent guanine N7 moieties. Binding is accompanied by large changes in specific imino, aromatic and methyl proton chemical shifts, indicating that a locally distorted structure forms at the binding site that affects the conformation of the two base pairs 3′ to the GGG sequence. The binding of Fe^{2+} to RGGG contrasts with that previously observed for the RTGR sequence, which binds Fe^{2+} with negligible structural rearrangements.

INTRODUCTION

DNA is sensitive to oxidative damage via the Fe^{2+}-mediated Fenton reaction:

$$Fe^{2+} + H_2O_2 + H^+ \rightarrow Fe^{3+} + H_2O + [OH]\cdot.$$

The DNA damage is characterized by a bimodal hydrogen peroxide dose–response curve with maximal damage occurring at ~1 mM H_2O_2 *in vivo*, and 0.05 mM *in vitro*, and a dose–response that is independent of H_2O_2 concentration at higher concentrations (1–3). The one or more highly reactive radical species that are produced by the Fe^{2+}-mediated Fenton reaction in the presence of DNA are kinetically distinguishable from free hydroxyl radical and are thus denoted by [OH]· (4). These species can damage DNA bases or cleave the DNA backbone by collapsing the deoxyribose ring (4). While the chemical identity of the oxidants produced in the presence of DNA is not established (except for a background of free OH produced in solution), DNA nicking at peroxide concentrations roughly <2 mM is quenched by H_2O_2 or ethanol, whereas that generated at higher H_2O_2 concentrations is resistant to both H_2O_2 and ethanol, and is 0th order with respect to peroxide concentration (5). The nicking at lower H_2O_2 concentrations is denoted as Mode I, whereas that at higher H_2O_2 concentrations is referred to as Mode II.

Henle *et al*. (6) have shown that in duplex DNA, purine–GGG (RGGG) and purine–TG–purine (RTGR) sequences are preferentially cleaved by Fe^{2+}-mediated Fenton reactions (cleavage sites are underlined). The RGGG sequences are the predominantly nicked species between 10 and 50 mM H_2O_2, while the RTGR sites are nicked at concentrations between 0.05 and 2.5 mM H_2O_2. Whereas four other sequences are cleaved to a lesser degree at the lower peroxide concentrations, RGGG is the only sequence that is preferentially cleaved at the higher peroxide concentrations. Unlike RTGR sequences that have a single site of cleavage, there is a gradation of nicking within RGGG sites with the more 5′ purine nucleotides in the sequence being nicked to a greater extent and the most 3′ nucleotide showing no preferential cleavage (6). Nicking mediated by Cu^{2+}/H_2O_2 as well as by SIN-1 (a nitric oxide mimic) and piperidine also occurs

*To whom correspondence should be addressed. Tel: +1 510 642 7583; Fax: +1 510 643 3388; Email: slinn@berkeley.edu
Present address:
Priyamvada Rai, Whitehead Institute for Biomedical Research, 9 Cambridge Center, Cambridge, MA 02142, USA

preferentially at the 5′ guanine relative to the 3′ guanines within a duplex TTAGGG context (7).

Preferential DNA damage within G-rich DNA sequences has potentially important biological implications. Mode II Fe^{2+}/Fenton oxidant-mediated nicking is preferentially localized to a $(TTAGGG)_{81}$ human telomere insert within plasmid DNA relative to other RGGG sequences found in the remainder of the plasmid (6). Interestingly, plasmids with and without the insert sustain a similar number of total nicks at RGGG residues by the Fenton oxidants, suggesting that telomeric DNA might act as a sink for iron-mediated oxidative damage. Recent studies have implicated cumulative oxidative damage at telomeres in cellular senescence and aging (8–11).

Preferential cleavage at RTGR during Mode I cleavage was explained by preferential localization of Fe^{2+} at the N7 position of the specific guanine within the RTGR sequence without a major distortion of the target site (12). The guanine N7 has the most negative electrostatic potential among the atoms of the DNA bases (13), though the total electrostatic potential varies depending on neighboring bases (14). Furthermore, relative to other DNA sequences, runs of guanine are thought to have unique properties with respect to both oxidative reactivity (15–18) and divalent transition metal cation association (14,19–22). The structural effects of transition metal association at RGGG and the broader issue of the different kinetic effects of H_2O_2 concentration upon preferential Fe^{2+}/H_2O_2-mediated cleavage have not been addressed. Therefore, using ^{1}H NMR, we have studied the interactions of Fe^{2+} with a 14 bp duplex, (5′ CGAGTTAGGGTAGC 3′)/(5′ GCTACCCTAACTCG 3′) and several variations within the AGGG segment. The data indicate that the pattern of preferential Fe^{2+}/H_2O_2-mediated cleavage previously observed at RGGG correlates with the affinities of the three individual guanines for binding Fe^{2+}. Moreover, there appear to be two preferred subsites within AGGG, involving Fe^{2+} binding between two adjacent guanines with distortion of base pairs 3′ to the AGGG sequence. This structural alteration contrasts with the minimal changes observed for Fe^{2+} binding at the Mode I site, RTGR (12), and may provide an explanation for the kinetic differences in DNA nicking at Mode I and Mode II cleavage sites.

MATERIALS AND METHODS

Materials

NaCl (99.999% pure) was from Sigma-Aldrich. DNA oligonucleotides from Operon Technologies, Alameda, CA were purified to 99% purity by reverse-phase HPLC and were then dried from ammonia to remove residual triethylamine, resuspended in 1 M NaCl, and desalted on a Water's C18 Plus Sep-pak cartridge by washing with 1 M NaCl followed by ddH_2O, and eluting with 50% HPLC-grade methanol. After vacuum drying, samples were dissolved in 130 mM NaCl. The concentrations of the two complementary strands were initially determined by A_{260} readings using the molar extinction coefficients provided by Operon. The accuracy of these coefficients was then checked by the method of continuous fractions as follows: the two strands were combined in varying molar ratios to determine the ratio that corresponded to the greatest hypochromicity at A_{260}. Since this ratio tended to be 1:1 for all the duplexes used in this study, the complementary strands were combined in a 1:1 molar ratio, based on the initial A_{260} readings. Lack of extraneous small peaks in the aromatic and imino regions of the NMR spectrum confirmed the complete formation of the duplex.

For NMR, 500 µl samples varied from 0.3–1.32 mM duplex. All solutions contained 130 mM NaCl in D_2O (Cambridge Isotopes) or 90% ddH_2O/10% D_2O, pH 6.8–7.0.

$FeSO_4{\cdot}7H_2O$ and $ZnCl_2$ (99+%) were from Aldrich. $FeSO_4$ was dissolved in N_2-de-aerated ddH_2O inside of a glove bag or glove box that had been thoroughly purged with N_2. The solutions were further purged with N_2 for several minutes. The DNA samples were likewise purged with N_2 before and after the addition of $FeSO_4$ and the NMR tubes containing the Fe^{2+}-DNA samples were sealed with rubber septum caps.

NMR spectra

NMR data were collected at 298 K on a Bruker DRX 500 or 600 MHz spectrometer. For ^{1}H 1D spectra, either 8k or 16k points were acquired with 64 or 128 scans. Solvent saturation transfer to imino protons was determined using a 60 dB presaturation pulse at the water frequency for 750 ms during the recycle delay, followed by a gradient pulse and a 1–1 jump and return to suppress the solvent peak. In order to assess baseline imino proton resonance intensities, comparison was made to data collected without presaturation of the water signal.

^{1}H T1 data were acquired using 1D inversion-recovery with a WATERGATE sequence for solvent suppression. One-dimensional spectra were recorded for samples dissolved in 90% H_2O/10% D_2O for recovery delays of 1, 2, 5, 10, 20, 50, 75, 100, 200, 500, 750 and 900 ms and 1, 1.2, 1.5, 2, 5 and 10 s. T1 values were determined by using Kaleidagraph 3.0 to fit the peak intensities at the different recovery times using the equation:

$$M_Z(t) = M_Z(0)[1-2\exp(-t/\mathrm{T1})].$$

^{1}H NOE data were used to assign the resonances of the duplexes. NOESY spectra in D_2O used 64 scans with 512 t1 values and 2k complex points in t2 with TPPI mode quadrature. The spectral widths were 5000 Hz at 500 MHz or 6024 Hz at 600 MHz. The residual solvent signal was reduced by presaturation. NOESY spectra of samples in 90% H_2O/10% D_2O used 64 scans with 512 t1 values and 4k complex points in t2 with States-TPPI mode quadrature. Spectral widths of 10 000 Hz at 500 MHz or 13 514 Hz at 600 MHz were used. Gradients or a 1–1 jump and return sequence was employed for water suppression. NOESY experiments had a mixing time of 200 ms. NOESY spectra were also used to follow broadening of resonances at low Fe^{2+} concentrations, affording a better resolution than 1D spectra.

NMR data processing

Data were processed using FELIX 97.0 (Biosym). A 60° skewed sine bell (qsb) apodization was applied prior to FT. The 1D spectra were processed using a convolution difference at the carrier frequency to remove the residual HDO signal and by applying a polynomial baseline correction function. For 2D spectra, a 60° skewed sine bell (qsb) apodization was applied in t1 and a 60° squared sine bell (qss) apodization was applied in t2 prior to FT. For 2D homonuclear data, Facelift 2.1 was used for baseline correction after processing with FELIX.

Spectra used for the comparison of intensities in the presence and absence of metals were processed identically to avoid differences from processing.

Estimation of K_d values

Dissociation constants (K_d) for the Fe^{2+}–DNA complexes were estimated from the Fe^{2+}-dependent chemical shift of the G9 imino proton of the duplexes (12; Supplementary Figure S4).

Longitudinal proton relaxation data interpretation

Observed methyl proton T1 values along with fractional occupancies and calculated paramagnetic relaxation contributions were used to estimate the distance between Fe^{2+} and methyl groups in the duplexes. Assuming an iron-independent contribution to relaxation from proton–proton dipolar couplings and rapid exchange of Fe^{2+} between DNA oligomers, the increased relaxation from the presence of Fe^{2+} can be described as:

$$1/T1_{obs} = 1/T1_{free} + F_{bound}(1/T1_{Fe^{2+}}) \quad \mathbf{1}$$

where

$T1_{obs}$ is the observed longitudinal relaxation time in the presence of Fe^{2+},
$T1_{free}$ is the longitudinal relaxation time in the absence of Fe^{2+},
F_{bound} is the fraction of DNA oligomers with Fe^{2+} bound, and
$T1_{Fe^{2+}}$ is the paramagnetic contribution to relaxation from the Fe^{2+}.
Values for $T1_{Fe^{2+}}$ were estimated from the Solomon–Bloembergen equation (23,24):

$$1/T1_{Fe^{2+}} = \xi^2[7j(\omega_e) + 3j(\omega_H)] \quad \mathbf{2}$$

where $\xi^2 = 1/r^6_{\text{Fe-H}}\{2/15\ [(S)\ (S+1)]\ (\mu_0/4\pi)^2\ [\gamma_e\ \gamma_H\ h/2\pi]^2\}$.
For high-spin Fe^{2+} interacting with protons,

$$\xi^2 = \left(1.971 \times 10^{-43}\right)/r^6_{\text{Fe-H}} \quad \mathbf{3}$$

where $r_{\text{Fe-H}}$ is the distance between Fe^{2+} and the relaxing methyl proton.

Taking the correlation time for the Fe^{2+} paramagnetic electrons, τ_e, to be 10^{-12} s (25), the value of $[7\,j(\omega_e) + 3\,j(\omega_H)]$ can be calculated to be 9.316×10^{-12}. Therefore, for protons interacting with high-spin Fe^{2+}, the value of $r_{\text{Fe-H}}$ can be calculated from $T1_{Fe^{2+}}$:

$$1/T1_{Fe^{2+}} = \left(1.84 \times 10^{-54}\right)/r^6_{\text{Fe-H}}. \quad \mathbf{4}$$

RESULTS

Fe^{2+} localization at AGGG within a duplex oligonucleotide

A 14 bp DNA duplex containing an RGGG sequence (Figure 1) was used to study sequence-specific Fe^{2+} localization. Resonances of the duplex were assigned using standard NOESY data. Broadening of proton NMR signals was followed as Fe^{2+} was added to the duplex. For the initial experiments, very low concentrations of Fe^{2+} (ca. 0–10 μM or ca. 0.01 Fe^{2+} per duplex) were utilized so that selective broadening near the stronger binding sites could be followed. Subsequently, the Fe^{2+} was incrementally increased to a stoichiometry of ≈3 Fe^{2+} per duplex.

	1	2	3	4	5	6	7	8	9	10	11	12	13	14	
5'	C	G	A	G	T	T	A	**G**	**G**	**G**	T	A	G	C	3'
3'	G	C	T	C	A	A	T	C	C	C	A	T	C	G	5'
	28	27	26	25	24	23	22	21	20	19	18	17	16	15	

Figure 1. Sequence of the unmodified oligonucleotide used in this study. The AGGG Fe^{2+} binding site is underlined. Z substitutions for guanine were made replacing G8, G9 or G10, which are indicated in bold. A substitution of the G10:C19 pair by a T:A base pair was also made.

With the low Fe^{2+} concentrations, gradual and selective broadening was observed in the aromatic region (Figure 2A), particularly for the H8 resonances of the guanines. As Fe^{2+} was increased from 0 to 7 μM, the greatest broadening (barring end effects at G15) occurred for G8, followed by G9 and then G10 (Figure 2B). The relative order of broadening was also verified in NOESY spectra. Some shifting and broadening were also seen for other resonances, indicating that while the GGG sequence had the highest binding affinity, Fe^{2+} also binds other sites to some extent. As Fe^{2+} was increased to approximately stoichiometric amounts relative to the duplex concentrations, broadening of the G residues became extreme and significant effects on other aromatic resonances could be observed, particularly for the bases flanking AGGG as well as those on the opposite strand (Supplementary Figures S1 and S2). The gradual and continuous effects indicate that Fe^{2+} is in fast exchange among available binding sites on the DNA.

Shifts were also observed for some imino and thymine methyl resonances (Figure 3). The imino resonances of the guanines in the AGGG segment showed the greatest Fe^{2+}-dependent changes in shift, moving significantly upfield and broadening (Figures 3A and C). To investigate whether Fe^{2+} binding led to the loss of base pairing at the affected guanines, saturation transfer to solvent H_2O was examined (Supplementary Figure S3). Despite significant Fe^{2+}-dependent broadening, none of the AGGG guanine imino proton signals showed a substantial Fe^{2+}-dependent intensity decrease upon solvent signal saturation, indicating that base pairing is retained. The imino proton resonance of T17 did show some Fe^{2+}-dependent increase in exchange, but the effect was relatively small.

The T17 methyl proton resonance also shifted significantly downfield upon Fe^{2+} addition (Figures 3B and C). T11, immediately 3′ to G10, showed Fe^{2+}-dependent broadening but underwent only a small chemical shift change. The methyl proton resonance for T22, which is opposite to the A7 in AGGG, did not change significantly, and the T5 methyl proton resonance experienced slight upfield shifting as well as broadening, probably due to some binding of Fe^{2+} at G4. The T6 and T26 methyl resonances were not significantly affected (Figure 3B). All Fe^{2+}-dependent shifts were reversed by addition of the Fe^{2+} chelators 2′,2″-bipyridyl or 1,10-phenanthroline (data not shown).

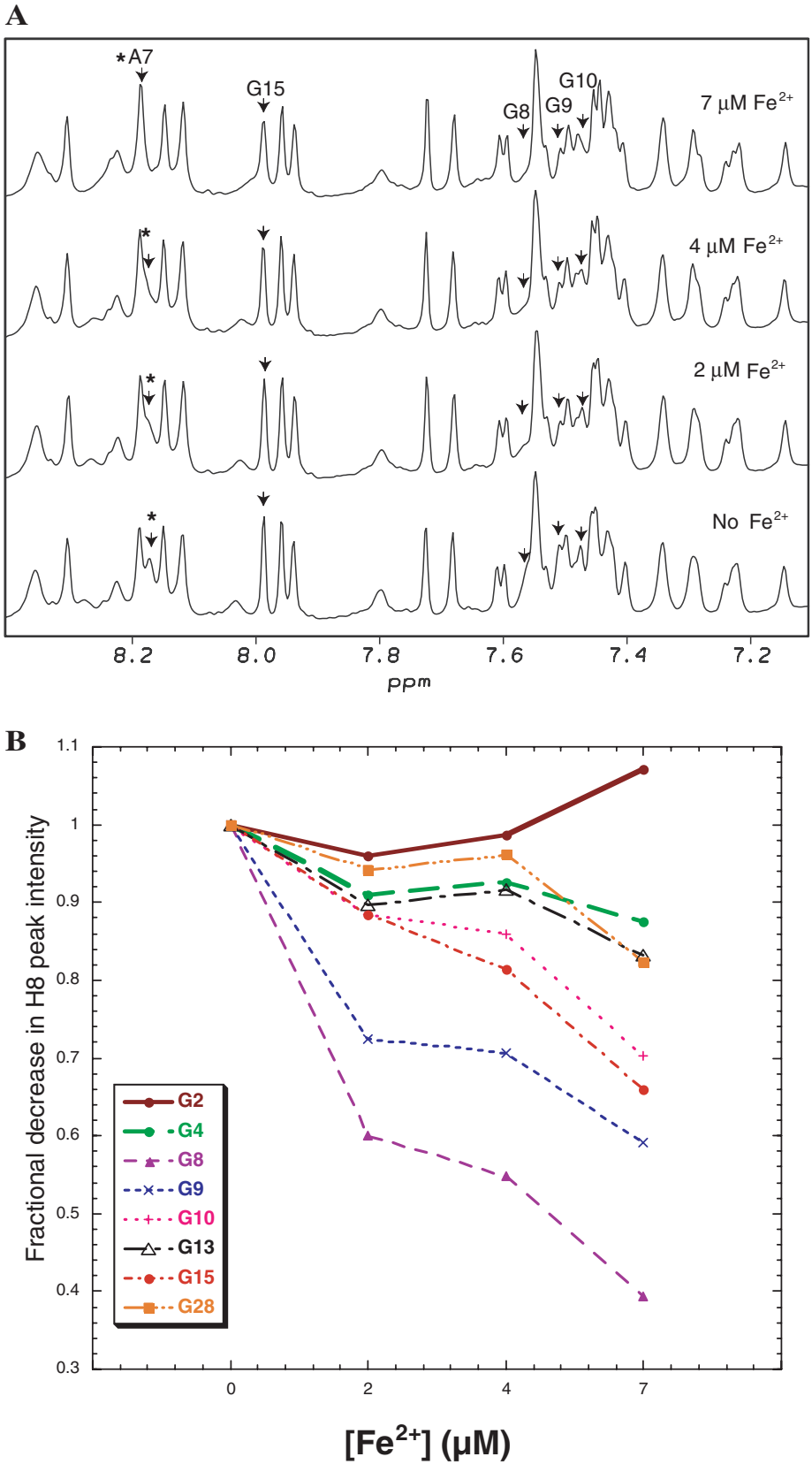

Figure 2. Fe^{2+}-mediated broadening of guanine H8 proton NMR signals in the AGGG duplex. (**A**) Aromatic (H6/H8) region from the ^1H NMR spectra of Fe^{2+} titration with a 1 mM sample of the AGGG duplex in 130 mM NaCl and 90% H_2O/10% D_2O. Fe^{2+} concentrations are indicated to the right of the spectra. Arrows indicate the preferential broadening among guanine H8 proton resonances and asterisks (*) indicates shifting of the A7 H8 proton (**B**) Graph of fractional decrease in guanine H8 proton signal intensity as a function of Fe^{2+} concentration. Peak intensity was measured using the cursor in FELIX 97.0.

Using the magnitude of chemical shift changes for the G9 imino proton as a function of Fe^{2+} concentration, a dissociation constant (K_d) of 2 mM was estimated for Fe^{2+} binding at the AGGG sequence (Supplementary Figure S4). This value is similar to the K_d of 0.9 mM, which was estimated for the binding of Fe^{2+} to the guanine of ATGA, within a duplex oligonucleotide (12). However, the chemical shift change observed at G9 upon addition of Fe^{2+} probably results from a combination of the interactions with the flanking guanines in AGGG, so this K_d value reflects the concentration of Fe^{2+} required to achieve half-maximal binding at AGGG as a whole rather than at a single guanine within the sequence.

Effects of modifications of the AGGG sequence upon Fe^{2+} binding

To investigate the possible presence of binding subsites within the AGGG sequence, Fe^{2+} binding to several related duplex oligonucleotides was probed. Three of these related oligonucleotides contained a single Z substitution at one of the three guanines in AGGG and are denoted as the AZGG, AGZG and AGGZ duplexes, respectively. In addition to lacking one guanine N7 as a binding site for the Fe^{2+}, these duplexes have different electrostatic characteristics at the GGG segment, owing to the replacement of the electronegative N7 with a neutral C7-H moiety. However, they are structurally similar as the positioning of the deazaguanine in the duplex and its stacking interactions are analogous to those of guanine. To assess the effect of the 'G stack' structure in AGGG on Fe^{2+} binding, the 3′ guanine base pair (G10:C19) was replaced by a T:A (T10:A19) base pair to give the AGGT duplex. This duplex is analogous to the AGGZ duplex in having only the 5′-pair of adjacent guanines but differs structurally, owing to the pyrimidine substitution for the 3′ guanine.

NMR spectra at multiple, micromolar range Fe^{2+} concentrations were collected with each duplex at roughly millimolar concentration. The observed selectivity in broadening indicates that the substitution of any one guanine did not abolish Fe^{2+} interactions with the other two guanines and the greatest broadening still occurred for the 5′ most guanine (Figure 4A–D). The H8 resonances of guanines G2, G4, G28 and G15 broaden more in the modified sequences than in the unmodified ones (Figure 4 versus Figure 2A), suggesting that the substitutions weaken binding in the AGGG segment consequently freeing Fe^{2+} to bind at weaker, alternative sites. Shifting and broadening occurred for the H8 of A7 in the AGZG, AGGZ and AGGT duplexes, reflecting Fe^{2+} binding at G8 (Figures 4B–D). However, in the AZGG duplex, the A7 H8 showed little Fe^{2+}-dependent broadening, while the shifting and broadening of the Z8 H8 resonance was similar to that of A7 H8 in the unsubstituted duplex, reflecting Fe^{2+} binding at G9 (Figure 4A).

The magnitude of Fe^{2+}-dependent chemical shift change for the methyl and imino proton resonances with 0.5 to 0.6 equivalents of Fe^{2+} per duplex for each of the duplexes are shown in Figure 3C. The imino protons are valuable markers for sensing conformational changes upon iron binding because there is one resonance for each base pair and these protons are away from the iron-binding site on guanine so that shifts are not likely to arise from direct paramagnetic effects of the metal. In the AZGG duplex, the Fe^{2+} induced shifts of the iminos are changed significantly relative to those for the AGGG duplex. The metal-induced shift of Z8 is opposite to that of G8, that of G9 is similar to that in the substituted sequence, but the effects at G10 and T11 are substantially increased, the shifts almost doubling in magnitude. These changes probably reflect the increased structural changes 3′ to the G9–G10 Fe^{2+}-binding site in this duplex, relative to duplexes containing the stronger affinity G8–G9 site.

For the AGZG duplex, the induced shift is enhanced at G8 but strongly reduced at Z9 and G10. This is consistent with G8 acting as an isolated site for Fe^{2+}-binding owing to the abolishment of adjacent guanine N7 sites. For the AGGZ duplex, the shift of G8 is dramatically enhanced, that of G9 was slightly enhanced, and that of Z10 was somewhat reduced, relative to G10 in the unmodified AGGG sequence. The change in shifting behavior reflects the loss of the weaker G9–G10 Fe^{2+} binding site and greater occupation of the G8–G9 site in the AGGZ duplex. However, the essential similarities in magnitude and direction of the induced shift in the AGGZ duplex and the unmodified duplex indicate that the G8–G9 pair is likely to be the predominant binding site in AGGG duplex, with a lesser contribution from the weaker affinity G9–G10 site.

The AGGT duplex might be expected to have binding capabilities similar to those of AGGZ. However, it showed enhanced shifts at G8 and T11, while the shift at G9 was almost the same as in AGGZ. These differences might reflect a conformational flexibility within the AGGT sequence, relative to the AGGZ sequence owing to the substitution of the 3′ pyrimidine.

Among the thymine methyl resonances, Fe^{2+}-induced shifts were quite small, except for that of T17 (Figure 3B). With the AZGG duplex, the Fe^{2+}-induced shift of T17 was enhanced relative to that in the AGGG duplex, probably because of enhanced Fe^{2+} binding at G9–G10 as reflected in the imino proton shifts. With the AGZG duplex, very little shift occurred, paralleling the pattern at Z9–G10. With the AGGZ duplex, the methyl region shift was the same as that for the AGGG duplex, paralleling the imino proton shifts. The T17 methyl shift is noticeably decreased (by almost a factor of two) for the AGGT duplex relative to the AGGZ duplex, (Figure 3C). Overall, the changes in the Fe^{2+}-dependent shift at the T17 methyl are likely to be indicative of structural rearrangements in the region 3′ to the G9–G10 binding subsite.

The Fe^{2+}-induced shifts for aromatic protons on the AGGG strand could not be followed for most of the protons in the binding site regions as they are severely broadened, and hence, provide limited information. It is worth noting, however, that in the AZGG duplex, Z8 H8 shifted 0.2 p.p.m. at 0.5 Fe^{2+} per duplex and broadened somewhat, but Z9 H8 in the AGZG duplex and Z10 H8 in the AGGZ duplex did not shift or broaden significantly in the individually substituted duplex oligonucleotides (Supplementary Figure S2). This observation is consistent with local structural perturbations occurring around the strongest affinity binding site (consisting of the G8–G9 pair), which bring the 5′ purine closer to the bound Fe^{2+}. A similar shifting and broadening behavior is seen for A7 H8 in the unmodified duplex, suggesting that the strongest affinity binding site at G8–G9 in AGGG may involve contributions from the 5′ A7 residue.

Shift changes in the CCCT strand could be followed, and generally paralleled the patterns described above. The notable exception was the H6 of T11 in the AGGT duplex, which exhibited more than three times the shift seen in the AGGG duplex (Supplementary Figure S2), indicating perhaps greater conformational flexibility in the region 3′ to the G8–G9 binding site owing to the presence of two adjacent pyrimidines (T10 and T11) in the AGGT duplex.

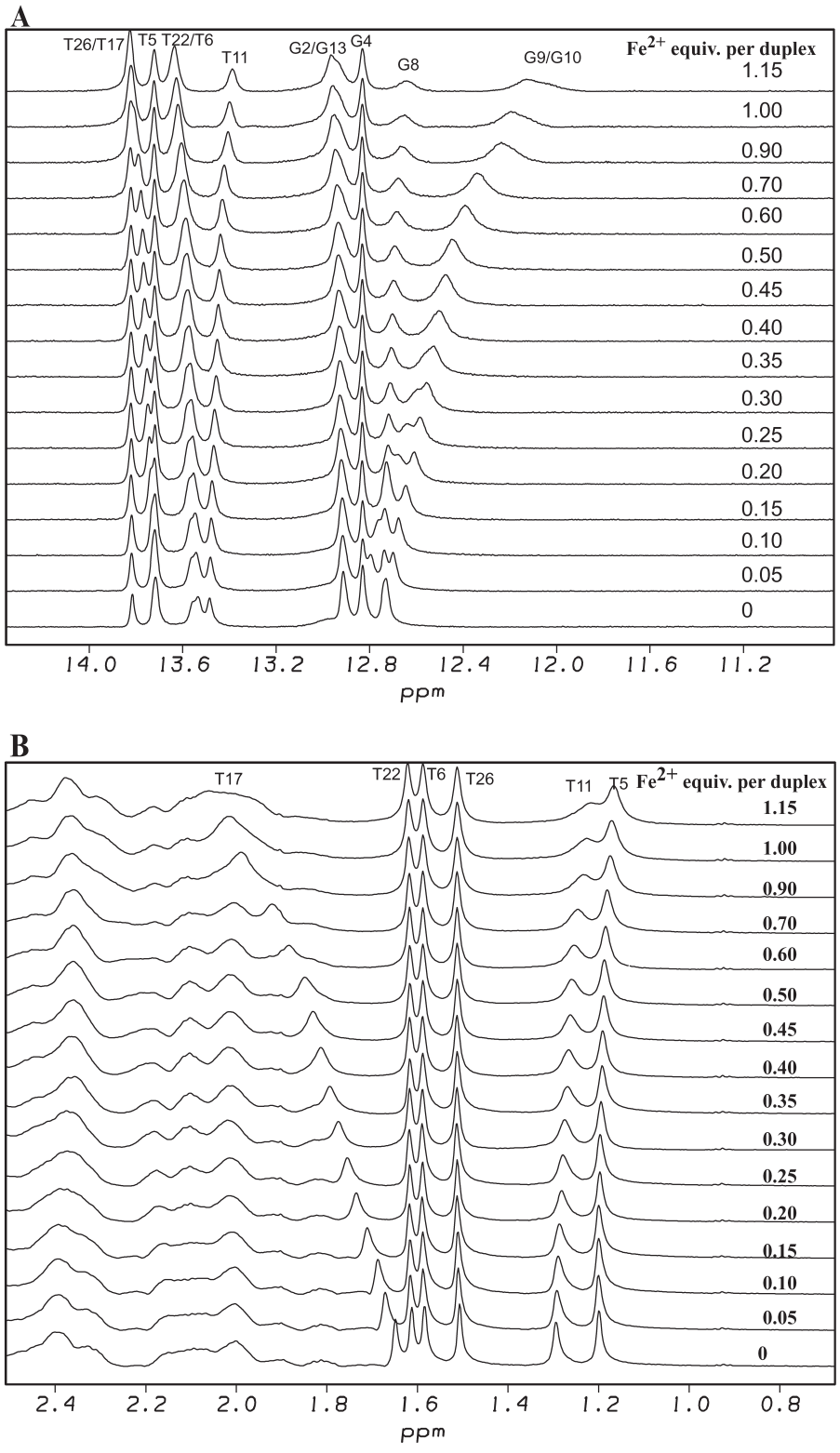

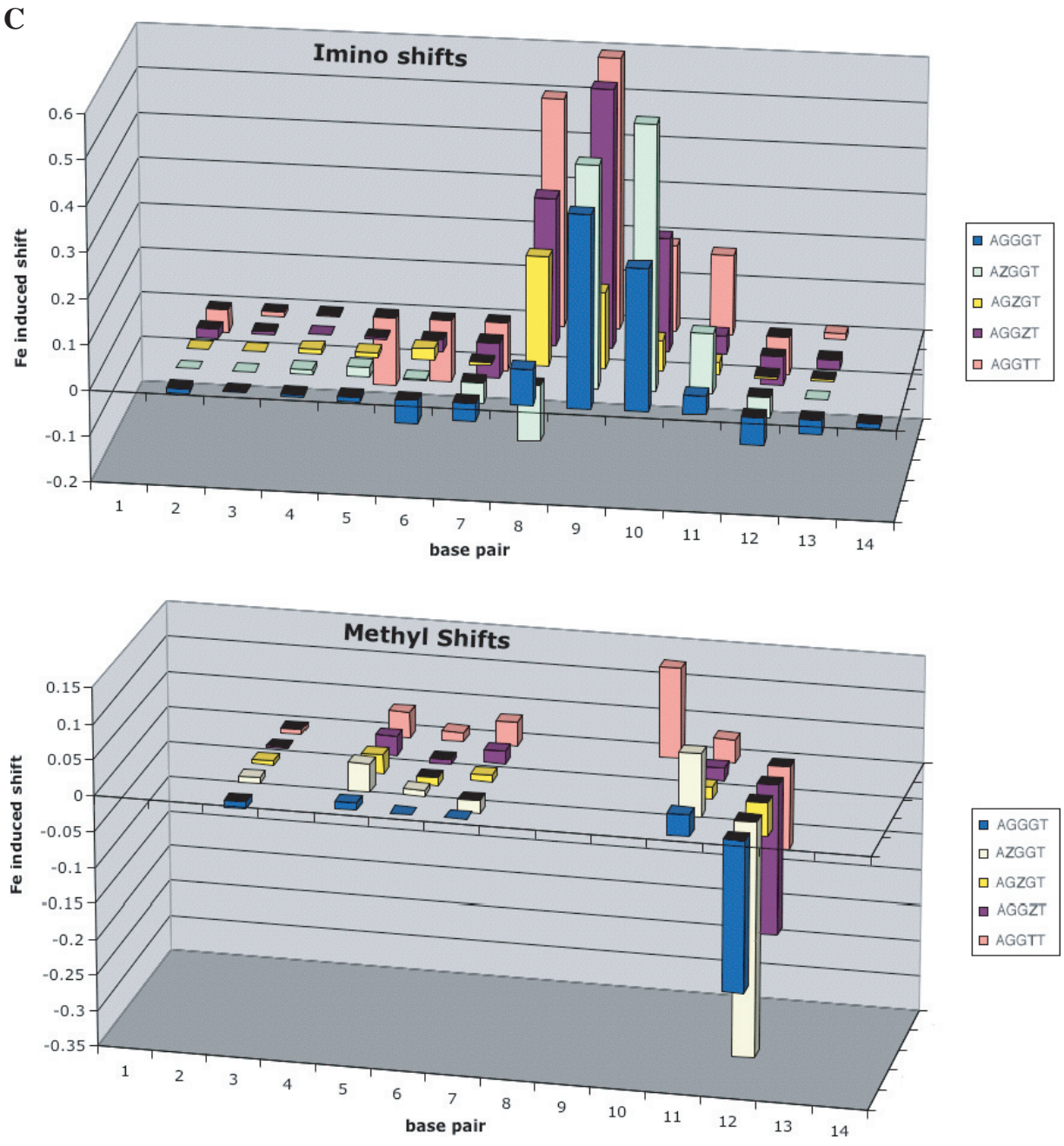

Figure 3. Fe^{2+}-dependent shifting of proton resonances within the AGGG duplex. $FeSO_4$ was titrated up to 1.15 equivalents per duplex as indicated, into a 0.65 mM sample in 90% H_2O/10% D_2O, 130 mM NaCl. (**A**) Imino resonances. (**B**) Methyl resonances. (**C**) Magnitude of changes in chemical shift resonances for the imino and methyl protons at 0.5 equivalents of Fe^{2+} per duplex for the AGGG, AZGG, and AGGZ duplexes and at 0.6 equivalents of Fe^{2+} per duplex for the AGZG and AGGT duplexes.

Probing Fe^{2+} binding by T_1 relaxation

Nuclear relaxation arising from electron–nuclear dipolar interactions depends on the inverse sixth power of the distance between the nucleus involved and the metal. Because of this strong distance dependence, nuclear spin–spin and spin–lattice relaxation are dominated by the closest occupied metal sites, even if that occupancy is relatively low. Iron binding at a purine followed by a thymine puts the thymine methyl ~4 Å from the Fe^{2+} in B-form DNA, while the methyls of thymines at next neighbor sites or on the opposite strand are >8Å from the Fe^{2+} and hence, much more slowly relaxed (<2% of the rate). Measurements for methyl protons produce relatively strong signals so that relaxation can be measured even when the lines are significantly broadened at high Fe^{2+} concentration. Figure 5 shows the paramagnetic contribution to relaxation ($R1_{total}$–$R1_{diamag}$) for the thymine methyls in the AGGG duplex and in the 7-deazaguanosine-substituted variants with 0.25 Fe^{2+} per duplex. In the unmodified duplex, the most strongly relaxed methyl was that of T11, which can be attributed to occupancy of the G10 N7 by Fe^{2+}. However, the

paramagnetic contribution was very small relative to that expected for full occupancy of the G10 N7 by Fe^{2+}. This fact, along with the strong broadening and shifts of A7, further support the preferential binding at the G8 or G9 in the run of G residues. Relaxation of the T5 methyl (which results from occupancy of G4) was only slightly elevated relative to that of T26, T6 and T22, which do not have nearby purines. A somewhat elevated relaxation of the T17 methyl probably arises from a combination of occupancy at G10 (discussed further below) and at G15 (the terminal base which has somewhat stronger binding than an isolated internal G).

Substitution with Z at any of the G residues within the AGGG sequence or with T for G10 enhanced the relaxation of T5 by 4- to 5-fold. Since the substitutions are far from T5,

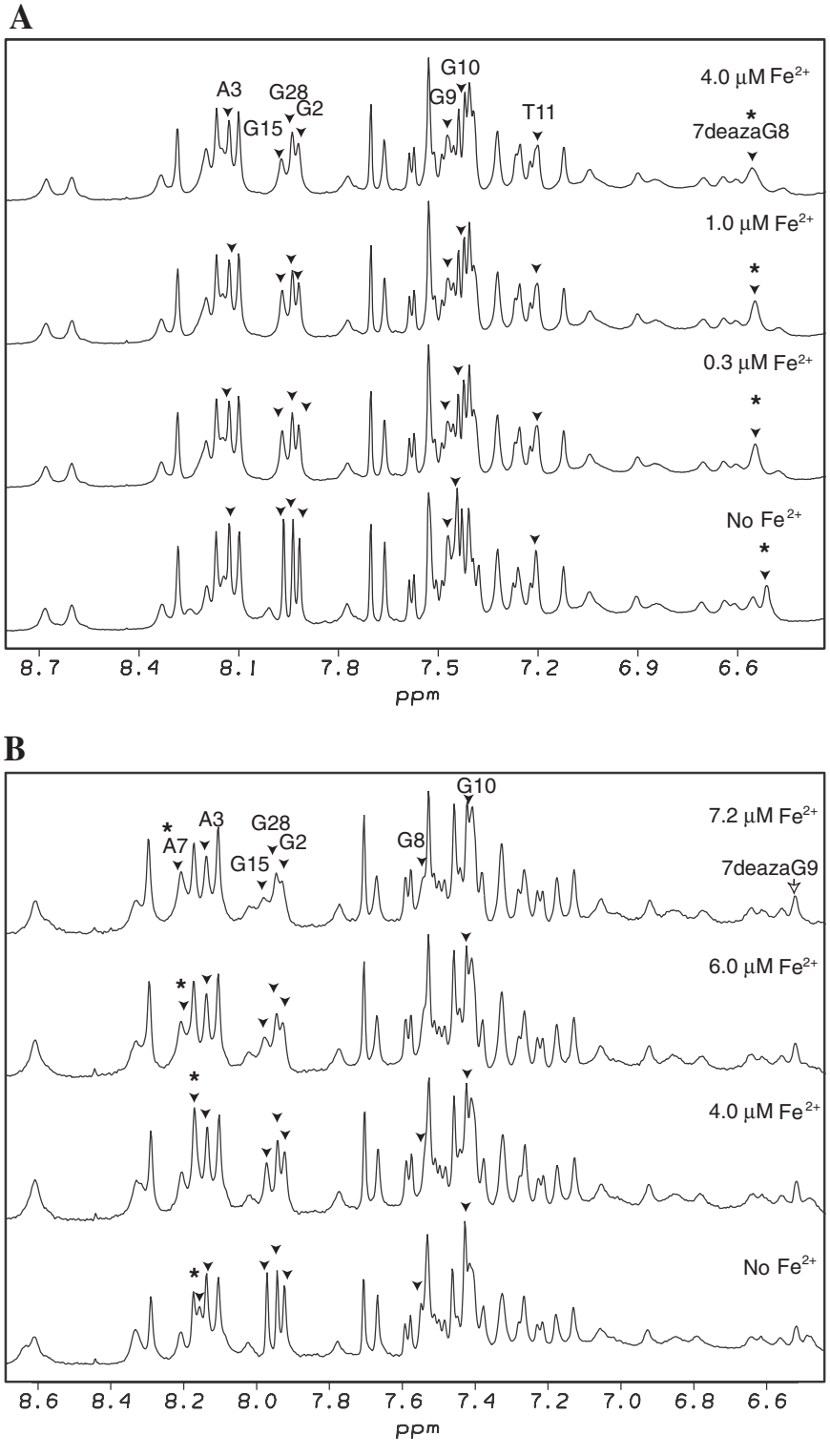

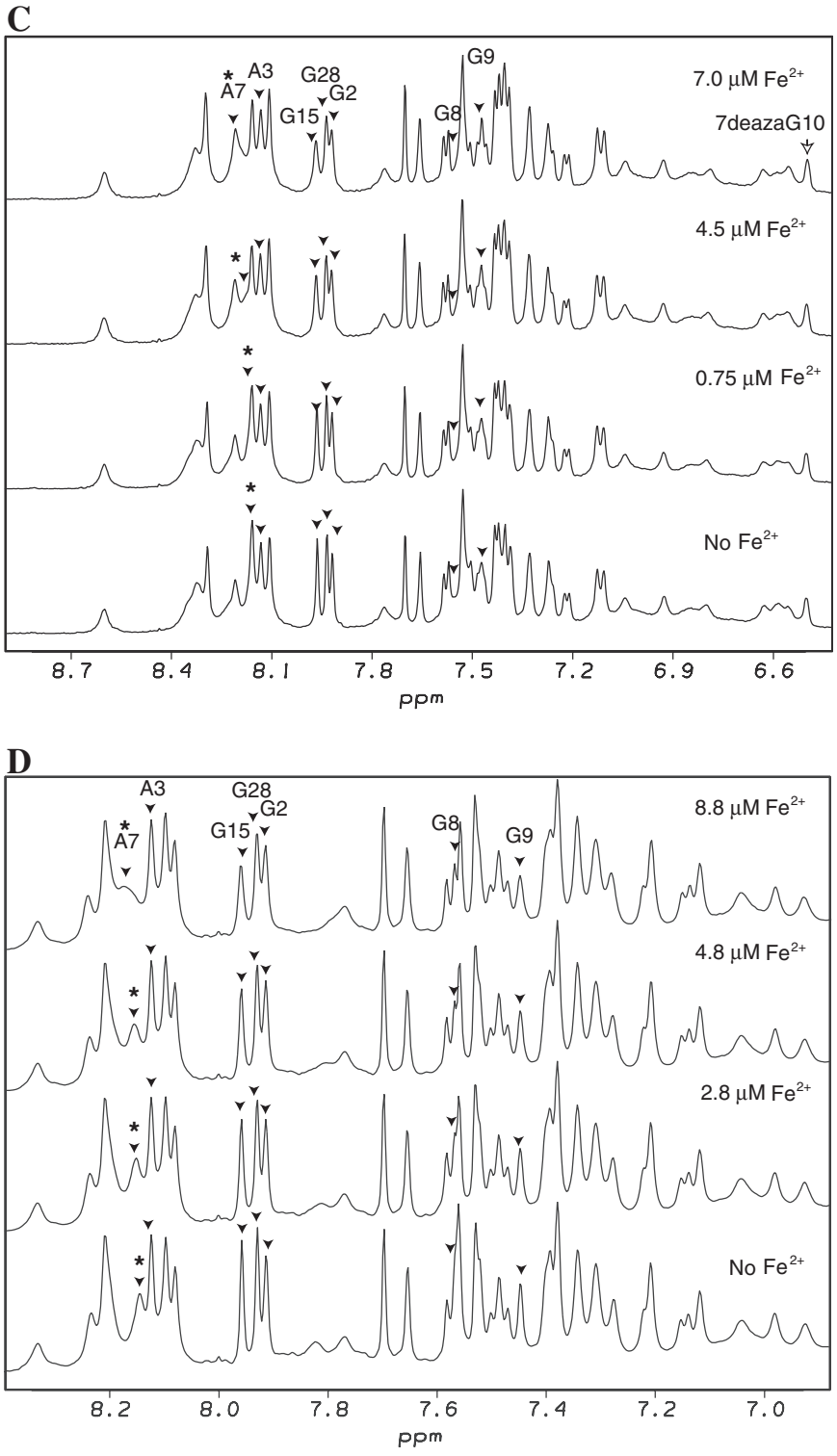

Figure 4. Aromatic (H6/H8) region from ^{1}H NMR spectra of Fe^{2+} titrations of modified duplexes. All samples were in 90% H_2O/10% D_2O and contained 130 mM NaCl. Fe^{2+} concentrations are indicated at the right of the spectra. Filled arrows indicate preferential broadening, asterisks (*) indicate shifting among aromatic proton resonances, and non-filled arrows indicate the Z H8 proton resonances. (**A**) 0.68 mM AZGG duplex. (**B**) 0.3 mM AGZG duplex. (**C**) 0.5 mM AGGZ duplex. (**D**) 1.15 mM AGGT duplex.

this enhancement indicates that the binding within the substituted AGGG sequence is weakened, leaving more Fe^{2+} free to bind at G4. A similar effect was seen for the other thymines. When G8 was substituted with Z, there was a dramatic enhancement of the relaxation of T11. This enhancement reflects the higher occupancy at G9 and G10, approximately double that of the unmodified sequence, though with lower affinity than for the unmodified sequence, as judged by the

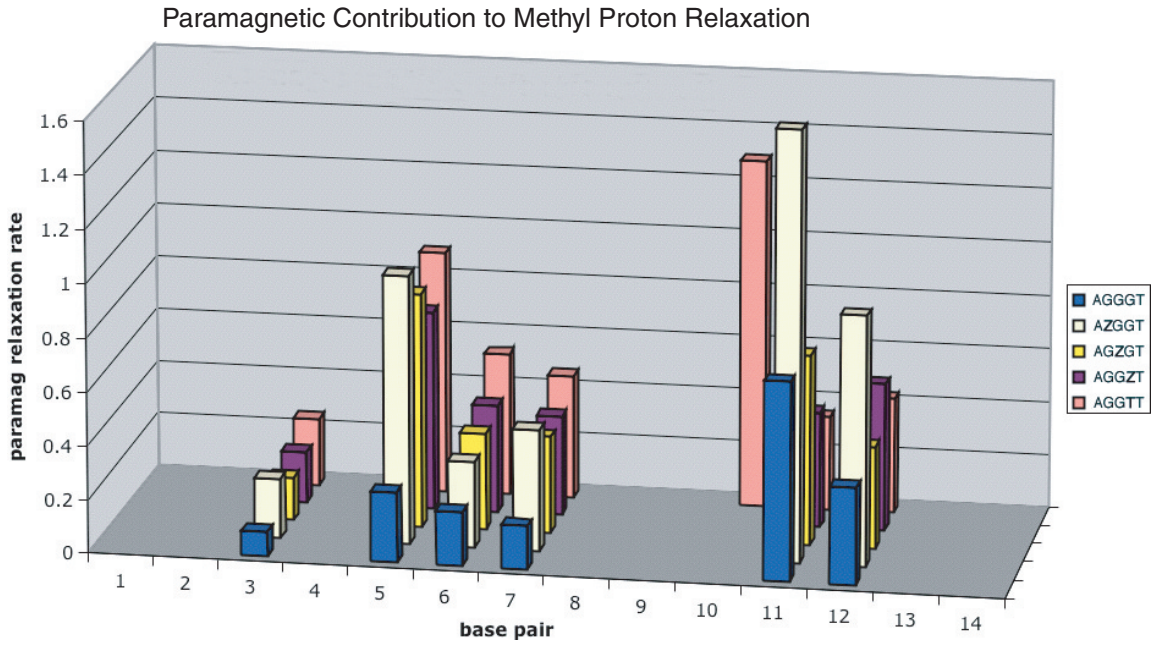

Figure 5. Fe^{2+}-mediated increase in thymine methyl proton longitudinal relaxation rates ($R1 = 1/T1_{para}$). Sample concentrations were: AGGG duplex, 0.5 mM; AZGG duplex, 0.68 mM; AGZG duplex, 0.3 mM; AGGZ duplex, 0.5 mM; and AGGT duplex, 0.5 mM. All samples were in 90% H_2O/10% D_2O, 130 mM NaCl and contained 0.25 equivalents of $FeSO_4$. The peak heights of the methyl proton resonances at the different recovery delays were measured using the cursor in the FELIX 95.0/97.0 program. These values were fitted to an exponential function from which the T1 values were calculated. Decrease in T1 is defined as T1 (no Fe^{2+})–T1 (Fe^{2+}).

reduced Fe^{2+}-dependent broadening and chemical shift changes (Figures 3 and 4).

With the AZGG duplex, the relaxation of T17 was also enhanced. This enhancement is partially explained by the higher occupancy of G10. However, the change in chemical shift of the T17 methyl proton resonances upon Fe^{2+} binding is also increased (Figure 3C), indicating a binding-induced distortion that changes the stacking of T17 with its neighbors, possibly bringing it closer to the iron bound at G10.

With the AGZG duplex that contains no adjacent GG residues, the relaxation of T11 dropped to a level similar to that of T5, each neighbored by an isolated G residue. With the AGGZ duplex, the T11 relaxation dropped to 'background' level (comparable to T6 or T22), which is consistent with the substitution removing the binding site at the 10th base. Substitution of G10 with T had basically the same effect on the relaxation of T11, but the new methyl on T10 was strongly relaxed, supporting a high occupancy at G9, a level similar to that seen in at T11 in the AZGG duplex. Overall, as expected, the T17 methyl proton T1 relaxation in the duplexes containing the G10Z or the G10T substitutions are rather similar, consistent with G8–G9 being the dominant Fe^{2+}-binding subsite that affects the relaxation behavior of the T17 methyl.

The results of paramagnetic relaxation measurements of the thymine methyl protons thus, confirm that Fe^{2+} binds preferentially within the GGG sequence with the highest affinity Fe^{2+} binding occurring at the 5′ dG within the GGG stretch. The relatively small change in T17 methyl relaxation coupled with the significant change in chemical shift (Figures 5 and 3C) provide further evidence of a downstream distortion transmitted from the binding site of the Fe^{2+}.

Zn^{2+} localization in the AGGG duplex

Zn^{2+} is diamagnetic and has been used to replace the paramagnetic transition metals, Co^{2+} and Mn^{2+} in NMR studies (21,26,27). If Zn^{2+} binding to the AGGG oligomer were to mimic that of Fe^{2+}, its substitution would allow for a better characterization of binding-induced structural changes because traditional NOE and coupling constant measurements would be feasible. Upon addition of Zn^{2+} to the AGGG-containing duplex, the magnitudes of chemical shift changes were much smaller than those induced by Fe^{2+} (Figure 6 versus Figure 3C; ~10-fold difference in the *y*-axis scale is to be noted), with the most prominent shifts being for the imino protons. Furthermore, the direction of shifts was reversed, though the relative sizes of shifts remained the same, relative to what was seen for Fe^{2+}, i.e. G9 > G10 > G8. Zn^{2+}-induced downfield shifts of imino protons in a TGGG site were reported previously, but with magnitudes G9 > G8 > G10 (using the same numbering) (22). The reason for this reordering is presumably contextual, since the study utilized a TGGG sequence as opposed to AGGG. No significant shifts were seen in the methyl region (Figure 6). The Zn^{2+}-induced chemical shifts did not approach limiting values even at 3 equivalents per duplex, indicating weaker binding than Fe^{2+} and preventing a quantitative assessment and precluding its use for structural analysis.

When Fe^{2+} was titrated into a sample with 3 equivalents of Zn^{2+}, the effects at 0.5 equivalents of Fe^{2+} (as judged by the broadening and changes in imino proton shifts) were equivalent to those without Zn^{2+} present, again indicating a much weaker binding by Zn^{2+} (data not shown). The fact that Zn^{2+}

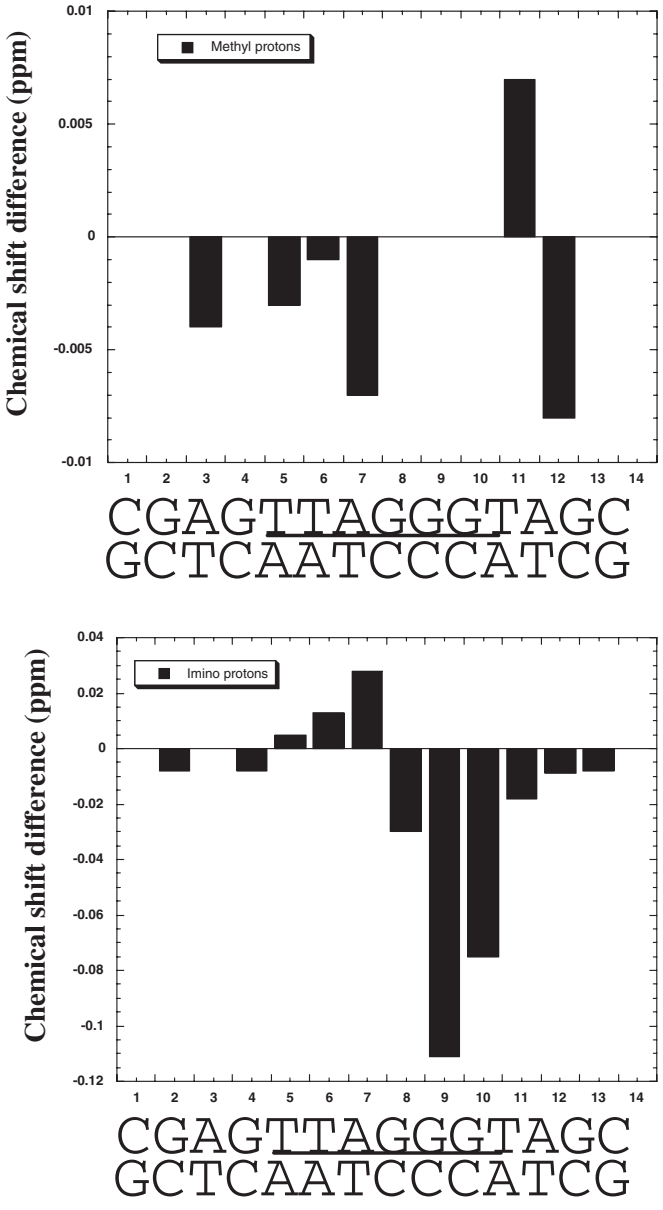

Figure 6. Changes in methyl and imino proton resonances in the AGGG duplex upon Zn^{2+} titration. Zn^{2+} was added up to 3 equivalents per duplex to a 0.5 mM duplex sample in 90% H_2O/10% D_2O and 130 mM NaCl. Magnitude and direction of Zn^{2+}-dependent changes in methyl and imino proton resonances at 3 equivalents of Zn^{2+} per duplex are shown. The difference in the *y*-axis scale relative to that of Figure 3C should be noted.

induces even small shifts in the GGG segment suggests that, in spite of the difference in preferred coordination geometry (tetrahedral for Zn^{2+} but octahedral for Fe^{2+}), the same features of this sequence (possibly electrostatic) are recognized by both Zn^{2+} and Fe^{2+}.

DISCUSSION

The patterns of chemical shift changes and paramagnetic relaxation induced in the AGGG duplex show that there is a preferential binding of Fe^{2+} at the run of three guanines. The broadening is most dramatic for the H8 resonances of the guanines, suggesting that the primary interaction of Fe^{2+} is in the major groove at the N7s. This suggestion is supported by the significant changes in binding behavior when deazaguanine is substituted for guanine, and is also consistent with crystallographic studies that have identified N7-metal chelation for Ni^{2+} (28,29). Of course, a secondary binding contribution from the guanine carbonyl group cannot be ruled out.

From the results of this study, we conclude that the previously observed preferential nicking by Fe^{2+}-mediated Fenton oxidants at the more 5′ nt in duplex RGGG sequences is mainly the result of higher Fe^{2+}-binding affinity at the more 5′ guanines in the sequence. However, this Fe^{2+} association includes the N7 positions of two adjacent guanines, as judged by H8 broadening and by the striking loss of Fe^{2+}-dependent shifts seen with the AGZG duplex, relative to those of the other four duplexes. The data also show that the 5′ guanine pair G8–G9 has a higher affinity than the G9–G10 pair. The requirement for a purine 5- to the G triplet might be structural, i.e. its stacking affects the detailed structure of the GGG segment so as to enhance the affinity.

Previous NMR studies with the paramagnetic transition metals, Mn^{2+} and Co^{2+}, indicated that these metals most significantly broaden the N7 (19) and H8 (21) NMR resonances of the 5′ guanines in GG runs in a DNA duplex. However, when the association of Mn^{2+} and Co^{2+} with GGG in a CGGGC context was studied (19), the central guanine exhibited the most pronounced broadening of the N7 signal. This led to the suggestion that the cations localize preferentially at the guanine with the highest occupied molecular orbital (HOMO), which would correlate with the lowest ionization potential. However, those conclusions depended strongly upon the signal-to-noise of the ^{15}N resonances, which appear to have been too low to allow for accurate line width determinations. Furthermore, there is a lack of consensus in *ab initio* calculations of HOMO distributions among GGG, as to which guanine correlates with the largest HOMO (30,31) and it is possible that the HOMO, and hence localization of transition metals on GGG, is affected by the sequence context of the guanines. Moreover, the association of transition metal cations at GGG stretches is complex and cannot be completely characterized by one isolated signal broadening. Finally, the effects seen with the other transition metals cannot necessarily be extrapolated to Fe^{2+}, since the coordination geometries and hydration shells of different transition metals can lead to differing patterns of association within DNA sequences (12,32).

The affinity of transition metals for runs of guanines is probably modulated by structural effects due to stacking among the purines and by electrostatic and orbital energy effects. The different contributions of these components are evident from the effects of Fe^{2+} localization in the AGGZ and AGGT duplexes. Each duplex contains a single consecutive guanine pair, but the AGGT duplex has a different structural conformation than the AGGG or AGGZ duplexes. This difference manifests itself as the slightly weaker binding of Fe^{2+} binding for AGGT relative to AGGZ and a different pattern of chemical shift changes. The minor role of pure electrostatics can also be seen from the difference in the binding of Zn^{2+} relative to Fe^{2+} at GGG. Zn^{2+} and Fe^{2+} have different ionic radii, preferred coordination geometries and *d*-orbital

occupancies, but the same net charge. Therefore, the similarity in relative site binding preferences (but not in absolute affinities) indicates that there is some role of the electrostatic profile in binding at GGG sequences, but other specific ligation effects must dominate, since Fe^{2+} binding is much stronger.

The structural changes induced by Fe^{2+} binding to the AGGG duplex are difficult to assess unambiguously owing to the rapid exchange of Fe^{2+} among the DNA molecules and among the guanines. The observed 'fast exchange' NMR behavior implies that, compared to the lifetime of the metal bound state, any structural change upon metal binding is rapid. Thus induced chemical shift changes (or any other NMR parameter) reflect a population-weighted average value. At high iron concentrations, metal-bound forms do become significantly populated, and thus considerably alter the observed chemical shifts. The sites with the largest shift changes in general must reflect the sites with the largest structural perturbations. When the chemical shifts from the AGZG duplex are compared to those from the duplexes that contain consecutive guanines, it appears that Fe^{2+} binding to GG pairs leads to significant chemical shift changes in and 3′ to the GG-containing region, consistent with a structural rearrangement. In contrast, H8 broadening with the AGZG duplex suggests isolated interactions at G8 N7 and, to a lesser extent, at G10 N7, leading to minor chemical shift changes that would not indicate a structural deformation. These observations reinforce the view that the binding site in AGGG involves two adjacent guanine N7 moieties.

The structural change around T17 upon Fe^{2+} binding (detected as chemical shift changes and enhanced relaxation) can be explained if such binding engenders movement of G8 and G9 that could 'ripple' further down the duplex. The strong downfield shift of the T17 methyl protons is consistent with the methyl group moving out from the major groove. Consistent with this observation, A12 also experiences fairly large chemical shift changes for its aromatic protons and significant chemical shift changes are also seen for T11, T17 and A18 aromatic proton resonances, lending further support for structural changes in the region 3′ to the AGGG site (Supplementary Figure S2).

At dGpC sites containing trimethylene interstrand crosslinks, which have significant distortions of base pair planarity in the region of the crosslink, the magnitudes of change in aromatic proton chemical shifts are approximately 0.7–0.8 p.p.m. (33). The changes in the aromatic region chemical shifts upon Fe^{2+} binding in this study were approximately 0.1–0.25 p.p.m. These shifts were observed at relatively low Fe^{2+} fractional occupancies (0.15–0.2); therefore, when extrapolated to the fully bound values, they are of comparable size to those induced by trimethylene crosslinking. Intrastrand cross-linking by cisplatin of a GGGTAC-containing duplex indicated that the longest-lived monoadducts formed, correspond to 3′ directional crosslinking being favored over 5′ directional crosslinking. These results led to the conclusion that this directional preference may be due to conformational changes induced in the GGTA stacking (34) and thus, may relate to our observations with the AGGG duplex regarding Fe^{2+}-mediated changes at base pairs 3′ to the binding subsites.

Although the lack of NOE-based structural restraints make it difficult to generate a model of Fe^{2+} binding to AGGG, we built a qualitative model starting from B-form sodium DNA by constraining the Fe^{2+} atom to be near the N7 atoms of G8 and G9 in an octahedral geometry (Figure 7). Under the energy minimization calculations, the G8 and G9 bases shifted slightly so as to bring their N7 atoms into the best orientation for Fe^{2+} binding. Interestingly, despite the lack of explicit restraints placed on it, the A7 base was significantly tilted in a 3′ direction in the major groove towards G8–G9, bringing its N7 moiety within ~3 Å of the localized Fe^{2+}. Such a distortion would be consistent with the pronounced broadening and shifting of the A7 H8 signal, which was observed at extremely low Fe^{2+} concentrations. This conformation of A7 leaves its N1 within hydrogen bonding distance (2 Å) of the T22 imino proton, in agreement with the relatively sharp imino proton signal of T22 even at >1 equivalents of Fe^{2+} per duplex.

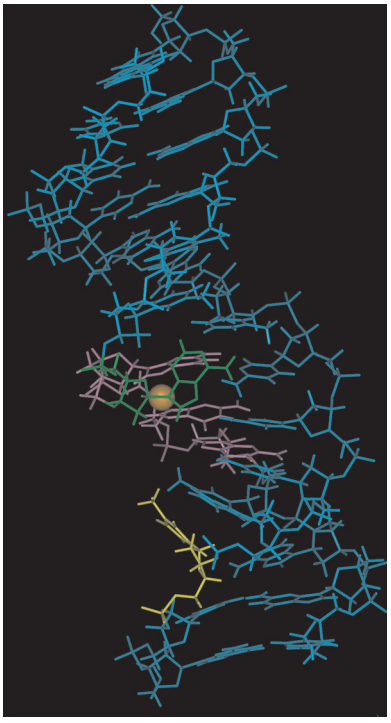

Figure 7. Model of Fe^{2+} association with the AGGG duplex. Molecular modeling was carried out on InsightII using the Discover module. T17 is shown in yellow, G8-G10 are in pink and A7 is in green. The sodium atoms used to neutralize the phosphate backbone during minimization are not displayed for clarity. The Fe^{2+} atom is placed between G8 and G9 N7 moieties and is shown in orange.

To assess the validity of the qualitative model in Figure 7, it was put into the chemical shift prediction program SHIFTS 4.1 (obtained from David Case's website at http://www.scripps.edu/mb/case/qshifts/about.htm). The relative order of the predicted base proton shifts for the native duplex agreed reasonably well with the observed shifts (Supplementary Table 1). Keeping in mind that the chemical shifts predicted by SHIFTS 4.1 are for a fully-bound complex, and that the observed shifts correlate to <0.5 fractional occupancy, the direction and general magnitude of observed shift changes predicted by SHIFTS 4.1 were consistent with the observed spectral shifts. In particular, the predicted shifts for the most perturbed moieties in the model, i.e. the A7 base protons (>0.25 p.p.m. downfield for H2 and H8) and T17 methyl

protons (>0.5 p.p.m. downfield; Figure 3B) were qualitatively similar to what is actually obtained upon Fe^{2+} titration.

The energy minimization model also suggests an explanation for the differences in the kinetics of cleavage by Fe^{2+} and H_2O_2 between the Mode II sequence, RGGG, and the Mode I sequence, RTGR. The modeled conformation of A7 places Fe^{2+} in closer proximity to the A7 C4′ than to the G8 C4′, which, in turn, is in closer proximity to Fe^{2+} than the G9 C4′. This order is consistent with the observed 5′ to 3′ preference polarity of Mode II cleavage at AGGG (6). The modeled geometry of A7 also helps enclose Fe^{2+} making it less solvent-accessible than at the Mode I RTGR site (12). This relative inaccessibility would explain the need for higher H_2O_2 concentrations for Mode II cleavage (6). Furthermore, once the Fe^{2+}/H_2O_2 complex is formed in the altered structure, the radical might be inaccessible to quenching agents, including a second H_2O_2 molecule, during the time-frame needed for reaction with the DNA.

The affinity of Fe^{2+} for binding at AGGG sequences may have a bearing on the role of oxidative DNA damage in telomere shortening and cellular senescence, since mammalian telomeres consist of TTAGGG repeats. In human fibroblasts, exposure to hydrogen peroxide induces telomere-shortening and premature cellular senescence (35,36). Significantly, hydrogen peroxide-induced senescence can be prevented by pre-treatment of fibroblasts with the iron-specific chelator, desferal (36). While telomeres are normally protected by telomeric binding proteins that stabilize the capped T-loop structure (37), it is possible that localization of endogenous ferrous ions during the stochastic open state might enhance telomere shortening under conditions of oxidative stress. Other experiments will be required to directly probe ferrous interactions in chromatin and telomeres in their cellular environment.

SUPPLEMENTARY MATERIAL

Supplementary Material is available at NAR Online.

ACKNOWLEDGEMENTS

The assistance provided by Dr Jeffrey Pelton with the NMR experiments and by Steven Damo in compiling SHIFTS 4.1 is gratefully acknowledged. This work was supported by NIH grants R01-GM19020 and P30-ES01896 (S.L.), and R01-GM43129 (D.E.W.) Funding to pay the Open Access publication charges for this article was provided by NIH grant R01-GM19020.

REFERENCES

1. Imlay,J.A. and Linn,S. (1988) DNA damage and oxygen radical toxicity. *Science*, **240**, 1302–1309.
2. Imlay,J.A., Chin,S.M. and Linn,S. (1988) Toxic DNA damage by hydrogen peroxide through the Fenton reaction *in vivo* and *in vitro*. *Science*, **240**, 640–642.
3. Kaneko,M. and Inoue,F. (1998) The sensitivity of DNA single strand breakage in mitochondria, but not in nuclei, of Chinese hamster V79 and variant cells correlates with their cellular sensitivity to hydrogen peroxide. *Toxicol. Lett.*, **99**, 15–22.
4. Koppenol,W.H. (1994) Chemistry of iron and copper in radical reactions. In Rice-Evans, C.A. and Burdon, R.H. (eds), *Free Radical Damage and Its Control*. Elsevier Science, pp. 2–24.
5. Luo,Y., Han,Z., Chin,S.M. and Linn,S. (1994) Three chemically distinct types of oxidants formed by iron-mediated Fenton reactions in the presence of DNA. *Proc. Natl Acad. Sci. USA*, **91**, 12438–12442.
6. Henle,E.S., Han,Z., Tang,N., Rai,P., Luo,Y.R.H. and Linn,S. (1999) Sequence-specific DNA cleavage by Fe^{2+}-mediated Fenton reactions has possible biological implications. *J. Biol. Chem.*, **274**, 962–971.
7. Oikawa,S. and Kawanishi,S. (1999) Site-specific DNA damage at GGG sequence by oxidative stress may accelerate telomere shortening. *FEBS. Lett.*, **453**, 365–368.
8. Saretzki,G. and von Zglinicki,T. (2002) Replicative aging, telomeres and oxidative stress. *Ann. N. Y. Acad. Sci.*, **959**, 24–29.
9. Kawanishi,S., Hiraku,Y. and Oikawa,S. (2001) Mechanism of guanine-specific DNA damage by oxidative stress and its role in carcinogenesis and aging. *Mutat. Res.*, **488**, 65–76.
10. Sozou,P.D. and Kirkwood,T.B.L. (2001) A stochastic model of cell replicative senescence based on telomere shortening, oxidative stress, somatic mutations in nuclear and mitochondrial DNA. *J. Theor. Biol.*, **213**, 573–586.
11. Jennings,B.J., Ozanne,S.E. and Hales,C.N. (2000) Nutrition, oxidative damage, telomere shortening, and cellular senescence: Individual or connected agents of aging?. *Mol. Genet. Metab.*, **71**, 32–42.
12. Rai,P., Cole,T.D., Wemmer,D.E. and Linn,S. (2001) Localization of Fe^{2+} at an RTGR within duplex DNA explains preferential cleavage by Fe^{2+} and H_2O_2. *J. Mol. Biol.*, **312**, 1089–1101.
13. Pullman,A. and Pullman,B. (1981) Molecular electrostatic potential of nucleic acids. *Quart. Rev. Biophysics*, **14**, 289–380.
14. Montrel,M., Chuprina,V.P., Poltev,V.I., Nerdal,W. and Sletten,E. (1998) Sequence-dependent binding of metal ion to DNA oligomers. A comparison of molecular electrostatic potentials with NMR data. *J. Biomol. Struct. Dyn.*, **16**, 631–637.
15. Hirakawa,K., Aoshima,M., Hiraku,Y. and Kawanishi,S. (2002) Photohydrolysis of methotrexate produces pteridine, which induces poly-G-specific DNA damage through photoinduced electron transfer. *Photochem. Photobiol.*, **76**, 467–472.
16. Murata,M. and Kawanishi,S. (2002) Oxidation of 5′-site guanine at GG and GGG sequences induced by a metabolite of carcinogenic heterocyclic amine PhI in the presence of Cu(II) and NADH. *Carcinogenesis*, **23**, 855–860.
17. Szalai,V.A., Singer,M.J. and Thorp,H.H. (2002) Site-specific probing of oxidative reactivity and telomerase function using 7,8-dihydro-8-oxoguanine in telomeric DNA. *J. Am. Chem. Soc.*, **124**, 1625–1631.
18. Kawanishi,S., Oikawa,S., Murata,M., Tsukitome,H. and Saito,I. (1999) Site-specific oxidation at GG and GGG sequences in double-stranded DNA by benzoyl peroxide as a tumor promotor. *Biochemistry*, **38**, 16733–16739.
19. Okamoto,A., Kanatani,K., Taiji,T. and Saito,I. (2003) ^{15}N NMR study on site-selective binding of metal ions to guanine runs in DNA: A good correlation with HOMO distribution. *J. Am. Chem. Soc.*, **125**, 1172–1173.
20. Martínez-Balbás,M.A., Jiménez-García,E. and Azorín,F. (1995) Zinc(II) ions selectively interact with DNA sequences present at the TFIIIA binding site of the *Xenopus* 5S-RNA gene. *Nucleic Acids Res.*, **23**, 2464–2471.
21. Frøystein,N.A., Davis,J.T., Reid,B.R. and Sletten,E. (1993) Sequence-selective metal ion binding to DNA oligonucleotides. *Acta Chem. Scand.*, **47**, 649–657.
22. Jia,X., Zon,G. and Marzilli,L.G. (1991) Multinuclear NMR investigation of Zn^{2+} binding to a dodecamer oligodeoxyribonucleotide: insights from ^{13}C NMR spectroscopy. *Inorg. Chem.*, **30**, 228–239.
23. Wengenack,N.L., Todorovíc,S., Yu,L. and Rusnak,F. (1998) Evidence for differential binding of isoniazid-resistant mutant KatG(S315T). *Biochemistry*, **37**, 15825–15834.
24. Todorovíc,S., Juraníc,N., Macura,S. and Rusnak,F. (1999) Binding of ^{15}N-labeled isoniazid to KatG and KatG(S315T): Use of two-spin [*zz*]-order relaxation rate for ^{15}N-Fe distance. *J. Am. Chem. Soc.*, **121**, 10962–10966.
25. Bertini,I. and Luchinat,C. (1996) In *Coordination Chemistry Reviews*, **150**, 77–110.
26. Frøystein,N.A. and Sletten,E. (1991) The binding of manganese(II) and zinc(II) to the synthetic oligonucleotide $d(C\text{-}G\text{-}C\text{-}G\text{-}A\text{-}A\text{-}T\text{-}T\text{-}C\text{-}G\text{-}C\text{-}G)_2$. A ^1H NMR study. *Acta Chem. Scand.*, **45**, 219–225.

27. Gochin,M. (1998) Nuclear magnetic resonance characterization of a paramagnetic DNA-drug complex with high spin cobalt; assignment of 1H and 31P NMR spectra, and determination of electronic, spectroscopic and molecular properties. *J. Biol. NMR.*, **12**, 243–257.
28. Abrescia,N.G.A., Malinina,L., Fernandez,L.G., Huynh-Dinh,T., Neidle,S. and Subirana,J.A. (1999) Structure of the oligonucleotide d(CGTATATACG) as a site-specific complex with nickel ions. *Nucleic Acids Res.*, **27**, 1593–1599.
29. Abrescia,N.G.A., Huynh-Dinh,T. and Subirana,J.A. (2002) Nickel-guanine interactions in DNA: crystal structure of nickel-d[CGTGTACACG]$_2$. *J. Biol. Inorg. Chem.*, **7**, 195–199.
30. Saito,I., Nakamura,T. and Nakatani,K. (2000) Mapping of highest occupied molecular orbitals of duplex DNA by cobalt-mediated guanine oxidation. *J. Am. Chem. Soc.*, **122**, 301–306.
31. Zhu,Q. and LeBreton,P.R. (2000) DNA photoionization and alkylation patterns in the interior of guanine runs. *J. Am. Chem. Soc.*, **122**, 12824–12834.
32. Gao,Y.G., Sriram,M. and Wang,A.H. (1993) Crystallographic studies of metal ion-DNA interactions: different binding modes of cobalt(II), copper(II) and barium(II) to N7 of guanines in Z-DNA and a drug-DNA complex. *Nucleic Acids Res.*, **21**, 4093–4101.
33. Dooley,P.A., Zhang,M., Korbel,G.A., Nechev,L.V., Harris,C.M., Stone,M.P. and Harris,T.M. (2003) NMR determination of the conformation of a trimethylene interstrand cross-link in an oligodeoxynucleotide duplex containing a 5′-d(GpC) motif. *J. Am. Chem. Soc.*, **125**, 62–72.
34. Villanueva,J.M., Jia,X., Yohannes,P.G., Doetsch,P.W. and Marzilli,L.G. (1999) Cisplatin (cis-Pt$(NH_3)_2Cl_2$) and cis-$[Pt(NH_3)_2(H_2O)_2]^{2+}$ intrastrand cross-linking reactions at the telomere GGGT DNA sequence embedded in a duplex, a hairpin, and a bulged Duplex: Use of Mg^{2+} and Zn^{2+} to convert a hairpin to a bulged Duplex. *Inorg. Chem.*, **38**, 6069–6080.
35. Petersen,S., Saretzki,G. and von Zglinicki,T. (1998) Preferential accumulation of single-stranded regions in telomeres of human fibroblasts. *Exp. Cell. Res.*, **239**, 152–160.
36. Chen,Q. and Ames,B.N. (1994) Senescence-like growth arrest induced by hydrogen peroxide in human diploid fibroblast F65 cells. *Proc. Natl Acad. Sci. USA*, **91**, 4130–4134.
37. Blackburn,E.H. (2002) Telomere states and cell fates. *Nature*, **408**, 53–56.